J. Fluid Mech. (1980), *vol.* 96, *part* 4, *pp.* 705–722
Printed in Great Britain

Solution of Howells' model of the scalar spectrum and comparison with experiment

By R. J. HILL

Wave Propagation Laboratory, Environmental Research Laboratories,
National Oceanic and Atmospheric Administration, Boulder, Colorado 80302

(Received 11 September 1979 and in revised form 8 January 1979)

Howells' model of the scalar spectrum for isotropic turbulent flow is simplified using a restriction to large Péclet number and statistically stationary turbulence at high wavenumbers, and is generalized by introducing Batchelor's constant as a free parameter. The resulting model is compared with data from the atmospheric surface layer, ocean, and liquid mercury. It is found that Howells' model, which is applicable for arbitrary Prandtl number (Pr), does not compare well with data for large and intermediate Pr at wavenumbers higher than those in the inertial–convective range. The model implies that the inertial–diffusive range asymptotic form, $k^{-\frac{1}{2}\gamma}$, cannot appear even for Pr as small as that of mercury ($Pr = 0{\cdot}018$).

1. Introduction

Howells (1960) obtained an approximate equation for the spatial spectrum of a conserved scalar quantity advected by turbulent flow. This equation is

$$\frac{\partial}{\partial t}\int_0^k \Gamma(n)\,dn + \left[\frac{1}{2}\int_0^k n^2 E(n)\,dn\right]^{\frac{1}{2}} k\Gamma(k) + 2\left[D^2 + \frac{4}{3}\int_k^\infty \frac{E(n)}{n^2}\,dn\right]^{\frac{1}{2}}\int_0^k n^2\Gamma(n)\,dn = 0, \tag{1}$$

where $\Gamma(k)$ is the scalar spectrum, $E(k)$ is the energy spectrum, t is time, k is the spatial wavenumber, the wavenumber is denoted by n when it is a variable of integration, and D is the diffusivity of the scalar. Equation (1) was constructed in such a way as to recover the inertial–diffusive range form, $\Gamma(k) \propto k^{-\frac{1}{2}\gamma}$, given by Batchelor, Howells & Townsend (1959) for small Prandtl numbers, as well as to recover the viscous–convective and viscous–diffusive range forms predicted by Batchelor (1959) for large Prandtl numbers. Consequently, Howells' equation (1) is applicable to the high-wavenumber range and for all Prandtl numbers. Hitherto, the solution of Howells' equation has not been given in the literature, possibly because of the complexity of equation (1). The solutions of a modified form of Howells' equation are studied herein and compared with observations. The modified Howells' equation is equation (6), which is derived from (1) by assuming that the Péclet number is large and that the turbulence is statistically stationary at high wavenumbers. Furthermore, Batchelor's constant is made a free parameter to be chosen by comparison with observations.

In order to observe an inertial–diffusive range, Clay (1973) has measured the spectrum of temperature fluctuations in turbulent liquid mercury. This data was recently compared with a model scalar spectrum developed by Hill (1978). Even though the

0022–1120/80/4385–8330 $02.00

Prandtl number is much less than unity ($Pr \simeq 0{\cdot}018$), the comparison of the data with that model spectrum indicated that no inertial–diffusive range can be observed in mercury because the transition to a viscous–diffusive range occurs at too low a wavenumber. Furthermore, the comparison indicated that no inertial–convective range (where $\Gamma(k) \propto k^{-\frac{5}{3}}$) was obtained in that data because the Péclet number was too small.

However, none of the scalar spectral models developed by Hill (1978) has a power law behaviour in the inertial–diffusive range. Consequently, it is of interest to solve Howells' equation in order to compare Clay's data with a model spectrum having the $k^{-\frac{17}{3}}$ power law. Furthermore, the accuracy of Howells' model can then be tested against data for the spectrum of temperature fluctuations in air ($Pr = 0{\cdot}72$) and temperature fluctuations in sea water ($Pr = 9{\cdot}2$).

2. The modified Howells' equation

The first term in equation (1) expresses the rate of loss of spectral content at wavenumbers lower than k caused by transfer to the higher wavenumbers. In (1) there is no scalar variance production; that is, the decay of the spectrum at low wavenumbers provides the input to the spectrum at high wavenumbers. The total rate of dissipation of scalar variance, χ, is given by

$$\chi = -\frac{\partial}{\partial t}\int_0^\infty \Gamma(k)\,dk.$$

Then equation (1) may be rewritten as follows:

$$-\chi - \frac{\partial}{\partial t}\int_k^\infty \Gamma(n)\,dn + G(k)\,\Gamma(k) + 2DN(k)\int_0^k n^2\Gamma(n)\,dn = 0, \tag{2}$$

where

$$G(k) \equiv kq^{-1}\left[2\int_0^k n^2 E(n)\,dn\right]^{\frac{1}{2}}, \tag{3}$$

$$N(k) \equiv \left[1 + (4b^2/3D^2)\int_k^\infty n^{-2}E(n)\,dn\right]^{\frac{1}{2}}. \tag{4}$$

The parameters q and b are introduced in equations (3) and (4); Howells' equation (1) corresponds to $b = 1$ and $q = 2$.

With a restriction to large Péclet numbers such that the variance-containing range and the diffusive dissipation range are well separated in wavenumber, then one may assume that scalar variance is provided at low wavenumbers at the rate χ such that a statistically steady state exists at high wavenumbers. In this case, for k sufficiently large

$$\frac{\partial\Gamma(k)}{\partial t} \simeq 0$$

and

$$\frac{\partial}{\partial t}\int_k^\infty \Gamma(n)\,dn \simeq 0.$$

When isotropy is assumed, χ is also the diffusive dissipation rate given by

$$\chi = 2D\int_0^\infty k^2\Gamma(k)\,dk.$$

With these restrictions, equation (2) may be written as

$$-\chi + G(k)\,\Gamma(k) + 2DN(k)\int_0^k n^2\Gamma(n)\,dn. \tag{5}$$

Equation (5) is now differentiated with respect to wavenumber and (5) is used to eliminate the dissipation integral. This procedure transforms Howells' equation into

$$\frac{d}{dk}[G(k)\,\Gamma(k)/N(k)] + \chi N(k)^{-2}\frac{dN(k)}{dk} = -2Dk^2\Gamma(k). \tag{6}$$

Kolmogorov scaling is now used; the energy dissipation rate ϵ and the kinematic viscosity ν give the dissipation wavenumber $k_d \equiv (\epsilon/\nu^3)^{\frac{1}{4}}$. The following notation is used for the non-dimensional quantities:

$$x \equiv k/k_d, \quad \tilde{G} = G/k_d^3\nu, \quad \tilde{\Gamma} = k_d^3\nu\Gamma/\chi, \quad \tilde{E} = E/k_d\,\nu^2.$$

In the inertial range of the energy spectrum

$$\tilde{E} = \alpha x^{-\frac{5}{3}}, \tag{7}$$

and in the inertial–convective range of the scalar spectrum

$$\tilde{\Gamma} = \beta x^{-\frac{5}{3}}, \tag{8}$$

where α is the Kolmogorov constant and β is the Oboukhov–Corrsin constant. In the inertial range ($x \ll 1$) the following approximations apply:

$$\tilde{G}(x) \simeq q^{-1}(\tfrac{3}{2}\alpha)^{\frac{1}{2}}x^{\frac{1}{3}}, \tag{9}$$

$$N(x) \simeq [1 + \tfrac{1}{2}b^2Pr^2\alpha x^{-\frac{2}{3}}]^{\frac{1}{2}}, \tag{10}$$

where $Pr = \nu/D$ is the Prandtl number. If, in addition, $k \ll k_c$, where $k_c = (\epsilon/D^3)^{\frac{1}{4}}$ is the Corrsin wavenumber, then

$$N(x) \simeq (\tfrac{1}{2}\alpha)^{\frac{1}{2}}bPrx^{-\frac{4}{3}}. \tag{11}$$

In the viscous range ($x \gg 1$) one has

$$\tilde{G}(x) \simeq x/q, \quad N(x) \simeq 1. \tag{12), (13}$$

By requiring that (8) satisfy (6) at sufficiently low wavenumbers that (9) and (11) apply, the parameter b is related to α, β and q by

$$b = 2[\beta^{-1}(2/3\alpha)^{\frac{1}{2}} - q^{-1}]/\sqrt{3}. \tag{14}$$

Equation (14) implies that, if $b = 1$, $q = 2$ and $\alpha = 1{\cdot}5$, then $\beta = 0{\cdot}5$. However, the review of observed β values by Hill (1978) suggests that β lies between 0·67 and 0·83. Therefore, Howells' model with $b = 1$ and $q = 2$ is abandoned; equation (14) is used to determine b from specified values of β, α and q.

Equation (6) is a first-order, linear, inhomogeneous differential equation. It may be solved by numerical integration. Alternatively, the Green's function method may be employed. In either case, the appropriate boundary condition is to require that $\tilde{\Gamma}$ satisfy equation (8) at a sufficiently low wavenumber, x_0, which lies in the inertial–convective range. The Green's function method gives the solution of (6) as

$$\tilde{\Gamma}(x) = \frac{N(x)}{\tilde{G}(x)}\left\{-\tfrac{3}{2}\beta Pr^{-1}x_0^{\frac{4}{3}}f(x_0, x) + N(x)^{-1} - 2Pr^{-1}\int_{x_0}^{x} x'^2 f(x', x)\,\tilde{G}(x)^{-1}\,dx'\right\}, \tag{15}$$

where

$$f(x_1, x_2) \equiv \exp\left[-2Pr^{-1}\int_{x_1}^{x_2} x'^2 N(x')\,\tilde{G}(x')^{-1}\,dx'\right].$$

The asymptotic forms of (15) are now discussed. The inertial–convective range consists of those wavenumbers such that $x \ll 1$ and $x \ll Pr^{\frac{1}{2}}$; that is $k \ll k_d$ and $k \ll k_c$. In the inertial–convective range equation (15) yields equation (8) as desired. In the limit $k \gg k_d$ and $Pr \gg 1$, equation (15) gives

$$\Gamma(k) = -\chi\gamma^{-1}k^{-1}\exp\left(Dk^2/\gamma\right), \tag{16}$$

where

$$\gamma = -q^{-1}(\epsilon/\nu)^{\frac{1}{2}}.$$

This result is Batchelor's theory for the viscous–convective and viscous–diffusive ranges. The parameter q is then identified as Batchelor's constant, and γ is an effective least-principal rate-of-strain parameter. The inertial–diffusive range occurs if $Pr \ll 1$ and consists of the wavenumbers such that $k \gg k_c$ and $k \ll k_d$. In the inertial–diffusive range equation (15) gives

$$\Gamma(k) = \tfrac{1}{3}b^2\alpha\chi\epsilon^{\frac{2}{3}}D^{-3}k^{-\frac{17}{3}}. \tag{17}$$

With $b = 1$, this is the result obtained by Batchelor *et al.* (1959). Howells' equation (1) was constructed in such a manner as to yield the asymptotic formulae in equations (8), (16), and (17).

3. Comparison of the modified Howells' model with experiments

Equation (6) is now solved by numerical integration, and the solutions are compared with the spectra of temperature fluctuations in air ($Pr = 0{\cdot}72$) observed by Champagne *et al.* (1977), in water ($Pr = 9{\cdot}2$) observed by Grant *et al.* (1968), and in mercury ($Pr = 0{\cdot}018$) observed by Clay (1973). Comparison of other scalar spectral models with these data and a more complete discussion of the experiments is given by Hill (1978).

Measurements yield the one-dimensional spectrum $\Psi(k)$ which is related to the three-dimensional spectrum $\Gamma(k)$ by

$$\Psi(k) = \int_k^\infty \frac{\Gamma(n)}{n}\,dn. \tag{18}$$

The Kolmogorov scaled one-dimensional spectrum $\tilde{\Psi}(x)$ is given by

$$\tilde{\Psi}(x) = k_d^3\nu\Psi(k)/\chi.$$

In the inertial–convective range (8) and (18) give

$$\tilde{\Psi}(x) = \beta_1 x^{-\frac{5}{3}} \tag{19}$$

with

$$\beta_1 = \tfrac{3}{5}\beta.$$

Equations (3), (4), and (6) constitute a model-dependent model, in that, one must have a model energy spectrum $E(k)$ to solve for $\Gamma(k)$. To obtain an $E(k)$ that closely resembles observations, a polynomial fit to the measured energy spectrum of Champagne *et al.* (1977) was used. The polynomial fit was kindly provided by F. H. Champagne. The polynomial was modified to satisfy equation (7) exactly for $x < 0{\cdot}14$, while

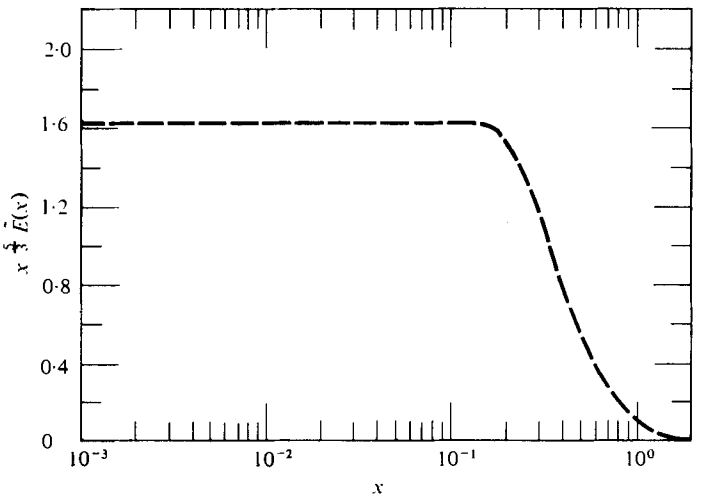

FIGURE 1. The energy spectrum to be used in equations (3) and (4).

causing only a slight change in the form of the dissipation range. The requirement that $1 = 2\int_0^\infty x^2\tilde{E}(x)\,dx$ was preserved in this transformation. The resulting energy spectrum to be used in equations (3) and (4) is shown in figure 1. The value of α is 1·62, which is slightly higher than most experimental values but is within experimental uncertainties.

3.1. *Temperature fluctuations in air*

The spectrum of temperature fluctuations measured in the atmospheric surface layer by Champagne *et al.* (1977) is now compared with the solution of (6). The temperature spectrum obtained by Champagne *et al.* (1977) has a 'bump' at high wavenumbers, as do the spectra measured by Williams & Paulson (1977) and by McConnell (1976). This bump is interpreted by Hill (1978) as being a tendency to a viscous–convective range at wavenumbers lower than those wavenumbers at which the diffusion of heat has a strong effect.

The one-dimensional spectrum is calculated from (6) and (18) and compared with the data obtained by Champagne *et al.* (1977) in figure 2. The calculations used $Pr = 0{\cdot}72$, and the experimentally observed value of $\beta_1 = 0{\cdot}41$. The cases $q = 7{\cdot}0$ and 80 are shown. A three-dimensional spectrum is calculated from a polynomial fit to the data of Champagne *et al.* (1977) and is compared in figure 3 with the $\Gamma(k)$ calculated from (6). The data and model spectra agree well for $x < 0{\cdot}02$ where equations (8) and (19) apply. However, they do not agree well at higher wavenumbers. The bump in the model spectrum always lies at higher wavenumbers than in the data. For $q = 7{\cdot}0$ the bump in the model spectrum has nearly the same height as in the three-dimensional 'data' spectrum of figure 3 whereas the $q = 7{\cdot}0$ model spectrum under-estimates the bump in the data on figure 2. On the other hand, the $q = 80$ model spectrum and the data in figure 2 have bumps with comparable heights. However, in figure 3 the three-dimensional model spectrum for $q = 80$ has a larger bump than does the three-dimensional spectrum derived from the data.

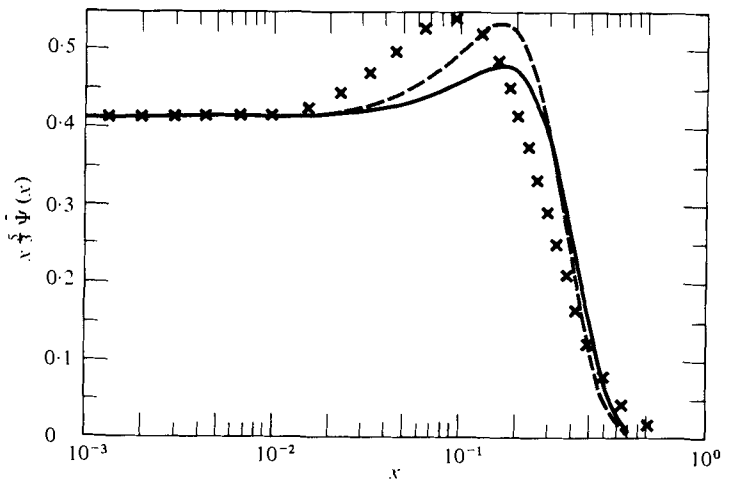

FIGURE 2. Howells' model compared with the data of Champagne *et al.* (1977); solid curve for $q = 7{\cdot}0$, dashed curve for $q = 80$; crosses indicate data points.

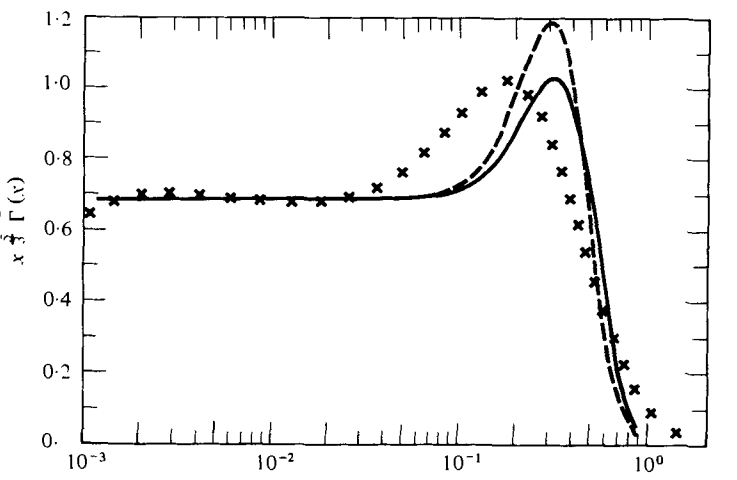

FIGURE 3. Howells' model compared with the three-dimensional temperature spectrum deduced from the data of Champagne *et al.* (1977); solid curve for $q = 7{\cdot}0$, dashed curve for $q = 80$; crosses indicate data points.

Values of q deduced from experiment lie between about 4·5 and 7·0 (Hill 1978), whereas Batchelor (1959) first estimated that q was about 2. The value $q = 80$ used in figures 2 and 3 is much higher than acceptable values.

The failure of equation (6) to reproduce the bump in the temperature spectrum in air is an intrinsic weakness of the model. The viscous–convective range in the model spectrum begins at too high a wavenumber. The effects of uniform straining on $\Gamma(k)$ calculated from (6) are strong only where $E(k)$ begins to decrease in its viscous dissipation range for $x \gtrsim 0{\cdot}14$. However, experiments show (Hill 1978) that the transition between the inertial–convective and viscous–convective ranges occurs at a much lower wavenumber, namely at x between about 0·06 and 0·04. Consequently Howells'

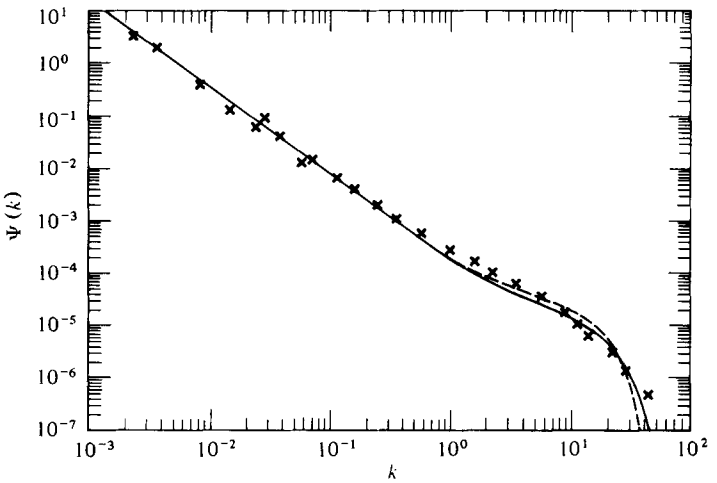

FIGURE 4. Howells model compared with the data of Grant *et al.* (1968); solid curve for $q = 8{\cdot}0$, dashed curve for $q = 80$; crosses are the data. Wavenumber k is in units cm^{-1}, and Ψ is in $(^{\circ}\mathrm{C})^{2}$ cm.

model will not adequately represent the scalar spectrum for $Pr \gtrsim 0{\cdot}4$ unless some function is introduced in place of $E(k)$ in equations (3) and (4) such that the new function decreases more rapidly than $x^{-\frac{5}{3}}$ for $x \gtrsim 0{\cdot}04$. Alternatively, one could replace the limits of integration in equations (3) and (4) with k multiplied by some factor so that more emphasis is given to the energy spectrum at wavenumbers greater than k. Such modifications are not considered here.

3.2. *Temperature fluctuations in the ocean*

Solutions of equation (6) are now compared with temperature spectra measured in a tidal channel by Grant *et al.* (1968), namely their run 2. For this run the values of the relevant parameters are: $\beta_1 = 0{\cdot}31$, $\epsilon = 0{\cdot}52$ cm^2 s^{-3}, $\chi = 4{\cdot}2 \times 10^{-3}\,^{\circ}\mathrm{K}^2$ s^{-1}, and $D = 1{\cdot}44 \times 10^{-3}$ cm^2 s^{-1}, so $Pr = 9{\cdot}2$, as is appropriate to their water temperature. In figure 4, the model one-dimensional spectra calculated using $q = 8{\cdot}0$ and 80 are compared with data points which are read from the graph given by Grant *et al.* (1968).

It is seen in figure 4 that the model curves make the transition from inertial–convective range to viscous–convective range at a higher wavenumber than in the data. This is the same defect that causes the discrepancy between the model spectra and the air-temperature data shown in figures 2 and 3. It is concluded that, for $Pr = 9{\cdot}2$ and any value of q, the model spectrum does not represent the data well for wavenumbers beyond the inertial–convective range. This problem is not peculiar to the use of the energy spectrum in figure 1 because solutions of (6) have this same feature when the energy spectrum given by Pao (1965) is used.

3.3. *Temperature fluctuations in mercury*

If the Prandtl number is very small but the Péclet number is very large then there exists an inertial–convective range followed by an inertial–diffusive range at higher wavenumbers; at yet higher wavenumbers the inertial–diffusive range is followed by a viscous–diffusive range. Howells' model places the transition from the inertial–diffusive to the viscous–diffusive range (for very small Prandtl number) at the same

Case	q	b	$\tilde{E}(x)$
1	2·0	0·455	$\alpha x^{-\frac{5}{3}}$
2	2·0	0·455	Figure 1
3	4·0	0·743	$\alpha x^{-\frac{5}{3}}$
4	4·0	0·743	Figure 1
5	8·0	0·888	$\alpha x^{-\frac{5}{3}}$
6	8·0	0·888	Figure 1
7	20	0·974	$\alpha x^{-\frac{5}{3}}$
8	20	0·974	Figure 1

TABLE 1. Parameters used to calculate the model spectrum of temperature fluctuations in mercury. All cases were calculated using $Pr = 0{\cdot}018$ and $\beta_1 = 0{\cdot}43$ so $\beta = 0{\cdot}717$

scaled wavenumber as the transition from inertial–convective to viscous–convective range (for very large Prandtl number). In the preceding it was found that Howells' model placed the transition between inertial–convective and viscous–convective ranges at too high a wavenumber for moderate to large Prandtl numbers. However, there is no *a priori* reason to believe that this implies that the transition from inertial–diffusive to viscous–diffusive range is wrongly positioned by Howells' model for very small Prandtl number. Thus, despite the failure of Howells' model to accurately describe the transition between the inertial–convective and viscous–convective ranges, the model may still accurately represent the inertial–diffusive range for $Pr \ll 1$, and the transition from the inertial–convective to the inertial–diffusive range, and the transition between the inertial–diffusive and viscous–diffusive ranges. For this reason it is of interest to compare Howells' model with the spectrum of temperature fluctuations in liquid mercury measured by Clay (1973).

The model scalar spectrum is calculated for the eight cases listed in table 1. For each value of q and b the spectrum was obtained using $\tilde{E}(x) = \alpha x^{-\frac{5}{3}}$ for all wavenumbers, even for $x > 0{\cdot}14$, as well as using the energy spectrum given in figure 1. Thus the odd-numbered cases used $\tilde{E}(x) = \alpha x^{-\frac{5}{3}}$ whereas the even-numbered cases used $\tilde{E}(x)$ from figure 1.

Figure 5 shows the functions $x^{\frac{5}{3}}\tilde{\Gamma}(x)$ and $x^{\frac{1}{3}\cdot 7}\tilde{\Gamma}(x)$. The curves for $x^{\frac{5}{3}}\tilde{\Gamma}(x)$ differ so slightly that only case 5 is plotted. Of course, $x^{\frac{5}{3}}\tilde{\Gamma}(x)$ tends to the constant β at small wavenumbers. The differences in $\tilde{\Gamma}$ for the eight cases are pronounced only at the higher wavenumbers and are evident in the curves for $x^{\frac{1}{3}\cdot 7}\tilde{\Gamma}(x)$.

In the odd-numbered cases for which $\tilde{E}(x) = \alpha x^{-\frac{5}{3}}$ was used, the function $x^{\frac{1}{3}\cdot 2}\tilde{\Gamma}(x)$ is seen to tend to a constant at the highest wavenumbers shown; this is the range where the asymptotic form in equation (17) applies. As b is decreased, equation (17) shows that $x^{\frac{1}{3}\cdot 2}\tilde{\Gamma}(x)$ tends to a smaller constant at high wavenumbers; consequently, in some cases in figure 5 the function $x^{\frac{1}{3}\cdot 2}\tilde{\Gamma}(x)$ has a local maximum.

In the even-numbered cases for which $\tilde{E}(x)$ is taken from figure 1, the curves for $x^{\frac{1}{3}\cdot 7}\tilde{\Gamma}(x)$ show no tendency to the asymptotic form in equation (17); these curves in figure 5 decrease monotonically at the higher wavenumbers. This monotonic decrease is the beginning of the viscous–diffusive range. Therefore, Howells' model predicts that no inertial–diffusive range where equation (17) applies can be observed unless Pr is much smaller than 0·018. This agrees with the analysis by Hill (1978) even though Howells' model places the transition from the inertial–diffusive range to viscous–

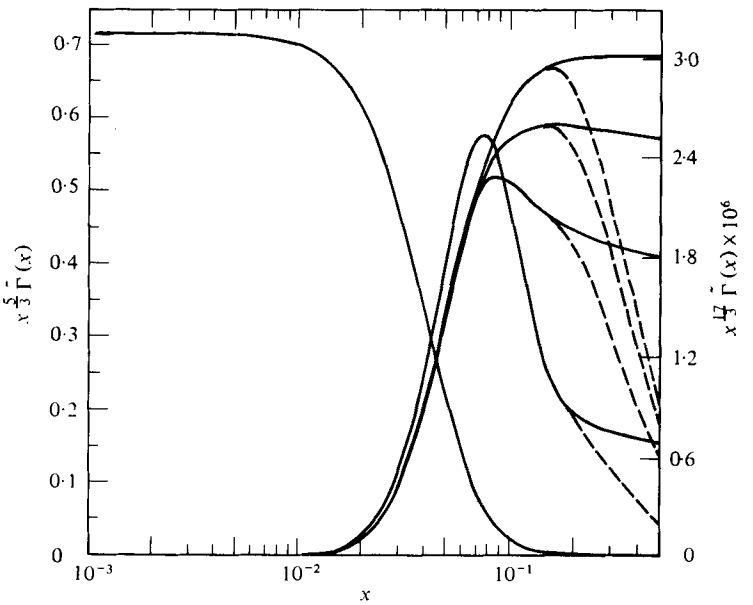

FIGURE 5. The three-dimensional spectrum from Howells' model for $Pr = 0{\cdot}018$ and the eight cases in table 1; $x^{\frac{5}{3}}\tilde{\Gamma}(x)$ asymptotes to $\beta = 0{\cdot}717$ on the left, whereas the curves for $x^{\frac{17}{3}}\tilde{\Gamma}(x)$ are on the right. From top to bottom along the right-hand side the solid curves are cases 7, 5, 3, and 1, whereas the dashed curves are cases 8, 6, 4, and 2.

diffusive range at a much higher wavenumber than do the models developed by Hill (1978).

The theory of the inertial–diffusive range as derived by Batchelor *et al.* (1959) yields

$$\Gamma(k) \propto k^{-4}E(k), \tag{20}$$

which in turn gives $\Gamma(k) \propto k^{-\frac{17}{3}}$ in the inertial–diffusive range where $E(k) \propto k^{-\frac{5}{3}}$. Batchelor *et al.* (1959) point out that one cannot extend equation (20) to the energy dissipation range because their mechanism for inertial–diffusive range spectral transfer is expected to become invalid where the energy spectrum decreases as rapidly as it does in the energy dissipation range. However, one can expect equation (20) to apply qualitatively to wavenumbers close to, but just beyond, the high-wavenumber end of the inertial range (e.g. for $0{\cdot}14 \leqslant x \lesssim 0{\cdot}3$ in figure 1). If this is so then equation (20) suggests that $\Gamma(k)$ must fall more rapidly than $k^{-\frac{17}{3}}$ as $E(k)$ enters its dissipation range; this is in agreement with the behaviour of the dashed curves in figure 5.

The function $x^{\frac{5}{3}}\tilde{\Psi}(x)$ and the dissipation spectrum $x^2\tilde{\Psi}(x)$ are shown in figures 6 and 7, respectively. The differences between the eight cases in table 1 are so slight at the lower wavenumbers that only case 5 is shown. The crosses and triangles in these and subsequent figures represent the temperature spectra in mercury measured by Clay (1973). The data giving the crosses and triangles were read from his figures 19 and 21 respectively, and were re-normalized to satisfy the requirement that the area under the scaled dissipation curve in figure 7 is $\frac{1}{6}Pr$ for $Pr = 0{\cdot}018$.

The data for the crosses and triangles were measured at grid Reynolds numbers $Re = 62000$ and 270000 respectively. The corresponding grid Péclet numbers are

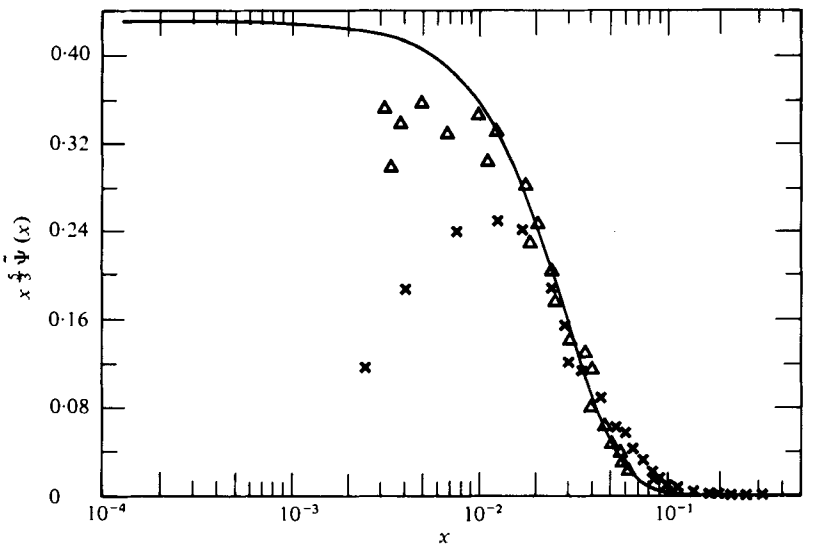

FIGURE 6. Comparison of Howells' model spectrum (solid curve) with the data (crosses and triangles) obtained by Clay (1973).

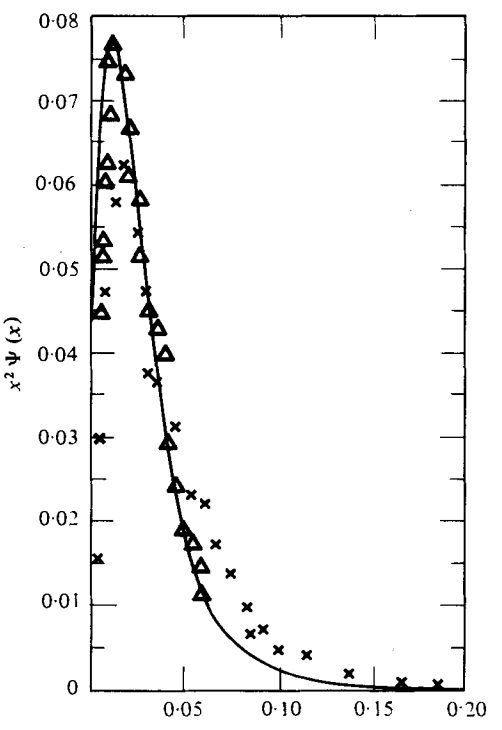

FIGURE 7. Comparison of the model dissipation spectrum (solid curve) with that from Clay's (1973) data (crosses and triangles).

therefore $Pe = Re \times Pr = 1120$ and 4860 respectively. Figure 6 shows that the model spectrum has its inertial–convective range at wavenumbers where the crosses show a variance-containing range. Thus the model suggests that the Péclet number of the run shown in figure 19 by Clay (1973) is too small to observe an inertial–convective range where equation (19) applies. This conclusion was also reached by Hill (1978) using the models given there. The $Pe = 4860$ run (triangles) attains greater values in figure 6 than does the $Pe = 1120$ run, which reinforces the conclusion that the $Pe = 1120$ run (crosses) has no inertial–convective range. Perhaps the $Pe = 4680$ run also fails to have a true inertial–convective range because the β values measured by Clay (1973) do not level off with increasing Reynolds number at the highest Reynolds numbers attained. The larger Péclet-number run (triangles) is in better agreement with the model spectrum (which corresponds to asymptotically large Péclet numbers) than is the smaller Péclet-number run (crosses).

The fall-off of the $Pe = 1120$ data in the variance-containing range causes the crosses to fall below the model spectrum at low wavenumbers in figure 6. This fall-off also causes the peak of the measured dissipation spectrum, crosses in figure 7, to be lower than for the model. Since the area under the data and model spectra must be $\frac{1}{6}Pr$ in figure 7, it follows that a lower peak in the measured dissipation spectrum requires the measured dissipation spectrum to exceed the model dissipation spectrum at higher wavenumbers. Thus, there is a Péclet-number effect such that measured values of the scaled spectrum $\tilde{\Psi}(x)$, at fixed scaled wavenumber x, must increase at the higher wavenumbers (tail of the dissipation spectrum) as the Péclet number decreases. This effect is illustrated in figure 7 by the fact that the $Pr = 1120$ data (crosses) lie above the $Pe = 4860$ data (triangles) at the highest wavenumbers. Unfortunately the $Pe = 4860$ data does not extend to yet higher wavenumbers because of amplifier noise limitations. Despite these problems caused by the close proximity of the variance-containing range, these and subsequent figures show that the model spectrum agrees with the crosses for $0{\cdot}02 < x < 0{\cdot}05$, and with the triangles for $0{\cdot}01 < x < 0{\cdot}06$.

Clay (1973) observed a k^{-3} power law over the limited range of wavenumbers $0{\cdot}025 < x < 0{\cdot}039$. A k^{-3} power law was predicted for the inertial–diffusive range by Gibson (1968). The function $x^3\tilde{\Psi}(x)$, obtained from the model, is compared with the data in figure 8. Of course, Howells' model is not expected to have a k^{-3} power law in the inertial–diffusive range. Whether or not the observed k^{-3} power law is real, the model curve in figure 8 suggests that with some scatter in data one could see a k^{-3} power law over a factor of 2 in wavenumber even if the power law did not exist. An entirely satisfactory observation of a k^{-3} power law would then require observing the power law over a wider range of wavenumbers.

The function $x^{1\cdot7}\tilde{\Psi}(x)$ is compared with the data in figure 9 for all eight cases in table 1. These curves are the one-dimensional analogue of the $x^{1\cdot7}\tilde{\Gamma}(x)$ curves in figure 5. In figure 9 the solid curves, for which $\tilde{E}(x) = \alpha x^{-\frac{5}{3}}$ was used, tend to the asymptotic inertial–diffusive range form $\tilde{\Psi}(x) \propto x^{-1\cdot7}$ at high wavenumbers. However, the dashed curves, for which the $\tilde{E}(x)$ in figure 1 was used, show a more rapid decrease at the highest wavenumbers because of the onset of the viscous–diffusive range. The data in figure 9 show a tendency to the asymptotic form $\tilde{\Psi}(x) \propto x^{-1\cdot7}$ at the high wavenumbers. The last datum at the top of the figure shows the presence of noise at yet higher wavenumbers. As mentioned previously, the $\Gamma(k) \propto k^{-1\cdot7}$ power law and consequently the $\tilde{\Psi} \propto x^{-1\cdot7}$ power law are not expected to be observed for $x \gtrsim 0{\cdot}14$ because the energy

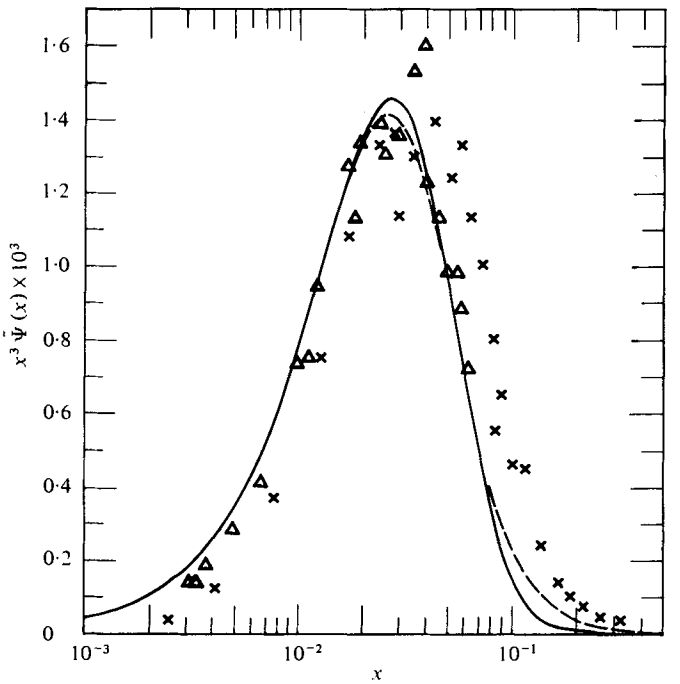

FIGURE 8. The function $x^3\tilde{\Psi}(x)$ for both Howells' model and Clay's data. Cases 1 and 2 are the solid curve; cases 7 and 8 are the dashed curve; crosses and triangles are data points.

spectrum in figure 1 is in its dissipation range. The energy spectrum in Clay's (1973) figure 19 ceases to obey $E(k) \propto k^{-\frac{5}{3}}$ for $x \gtrsim 0{\cdot}10$. Clay found the $x^{-\frac{17}{3}}$ power law to hold over the wavenumber range $0{\cdot}12 < x < 0{\cdot}23$. Because these wavenumbers exceed $x = 0{\cdot}10$, this is apparently not the $x^{-\frac{17}{3}}$ inertial–diffusive range predicted by Batchelor *et al.* (1959).

A striking feature in figure 9 is that the spectral level is much higher in the data than for the model curves at the high wavenumbers. One would need $b \simeq 1{\cdot}5$ for the model spectrum to match the data at these high wavenumbers. From equation (14), b cannot exceed 1·03 even as $q \to \infty$ for the values of β and α used here. To obtain $b = 1{\cdot}5$ one must use much smaller values of β and α than those used here. As previously noted, there is a Péclet-number effect such that, if the Péclet number is so small that the variance-containing and dissipation ranges are in close proximity, then measured values of $\tilde{\Psi}$ are larger at the highest scaled wavenumbers than for large-Péclet-number data. Is this Péclet-number effect sufficient to lower the crosses in figure 9 to the model curves in the limit that the variance-containing and dissipative ranges are well separated? A rough estimate can be obtained by taking a β_1 value from the peak of the crosses in figure 6 (i.e. $\beta_1 \approx 0{\cdot}25$ so $\beta \simeq 0{\cdot}42$) and substituting it into equation (14). With $\alpha = 1{\cdot}5$ and $q = 5{\cdot}0$ (the result is insensitive to the choice of q) this yields $b \simeq 1{\cdot}6$, which is close to the previous estimate of $b \simeq 1{\cdot}5$ necessary for Howells' model to match the data at the high wavenumbers in figure 9. Thus, Howells' model suggests that the Péclet-number effect is sufficient to lower the crosses in figure 9 to the model curves in the limit of large Péclet number. However, a definitive answer must await

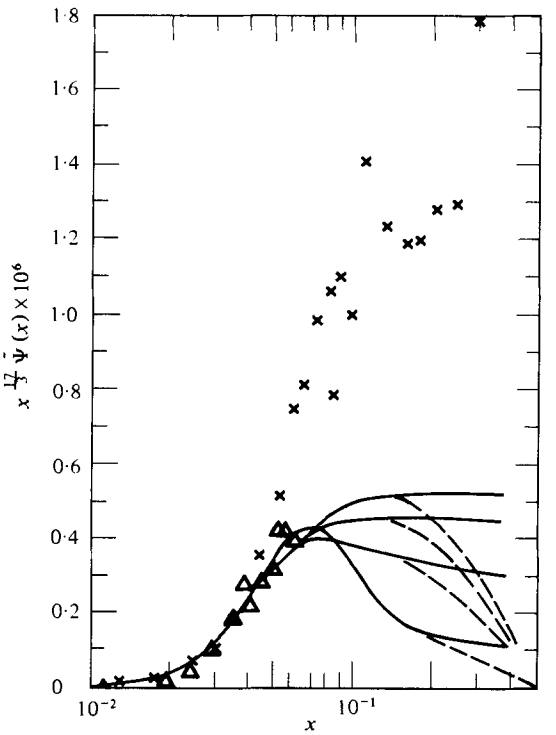

FIGURE 9. Comparison of $x^{\frac{1}{3}}\tilde{\Psi}(x)$ calculated from Howells' model for the eight cases in table 1 with Clay's data (crosses and triangles). From top to bottom along the right edge the solid curves are cases 7, 5, 3, and 1, whereas the dashed curves are cases 8, 6, 4, and 2.

large-Péclet-number experiments in mercury that can resolve wavenumbers as large as $x \approx 0{\cdot}2$. Unfortunately, the $Pe = 4860$ data do not extend to sufficiently large wavenumbers because of amplifier noise.

4. Strain-rate scalar-dissipation correlation

The 'strain-rate scalar-dissipation correlation coefficient' is defined by (Clay 1973)

$$\Sigma \equiv \overline{\left(\frac{\partial\theta}{\partial x_1}\right)^2 \frac{\partial u_1}{\partial x_1}} \Big/ \left[\overline{\left(\frac{\partial\theta}{\partial x_1}\right)^2}\,\overline{\left(\frac{\partial u_1}{\partial x_1}\right)^2}^{\frac{1}{2}}\right], \tag{21}$$

where θ is the scalar fluctuation, u_1 is streamwise velocity fluctuation, x_1 is the co-ordinate in the streamwise direction and the over-bar denotes averaging. The fluctuation in the rate-of-strain tensor is denoted by e_{ij}, that is

$$e_{ij} = \frac{1}{2}\left(\frac{\partial u_i}{\partial x_j} + \frac{\partial u_j}{\partial x_i}\right),$$

where i and j have values 1, 2, or 3 for the three spatial directions. Statistical isotropy gives the relationships

$$2\overline{e_{ij}\,e_{ij}} = 15\overline{(\partial u_1/\partial x_1)^2},$$

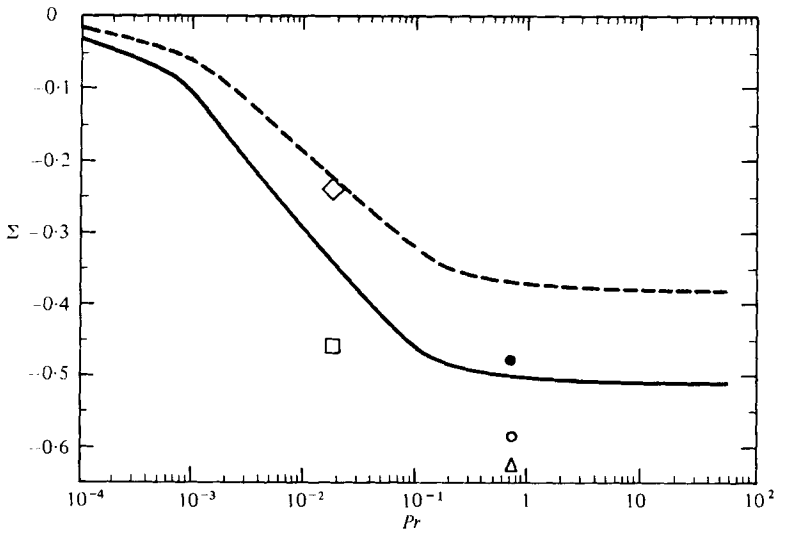

FIGURE 10. The correlation Σ as a function of Pr. Model 2 is the dashed curve; model 4 is the solid curve. □, Clay's (1973) $Pr = 0{\cdot}018$, $Pe = 1120$ data; ◇, Howells' (1960) model for $Pr = 0{\cdot}018$; ○, the 9-run average of Williams & Paulson (1977); ●, low-noise run, Williams & Paulson; △, Champagne *et al.* (1977).

$$\overline{\frac{\partial\theta}{\partial x_i}\frac{\partial\theta}{\partial x_i}} = 3\overline{(\partial\theta/\partial x_1)^2},$$

$$2\overline{\frac{\partial\theta}{\partial x_i}\frac{\partial\theta}{\partial x_j}\frac{\partial u_i}{\partial x_j}} = 2\overline{\frac{\partial\theta}{\partial x_i}\frac{\partial\theta}{\partial x_j}e_{ij}} = 15\overline{(\partial\theta/\partial x_1)^2(\partial u_1/\partial x_1)},$$

where repeated indices are summed. Thus Σ can also be expressed as

$$\Sigma = (\tfrac{8}{5})^{\frac{1}{2}}\overline{\frac{\partial\theta}{\partial x_i}\frac{\partial\theta}{\partial x_j}e_{ij}}\Big/\left[\overline{\frac{\partial\theta}{\partial x_i}\frac{\partial\theta}{\partial x_i}}\,\overline{e_{ij}e_{ij}}^{\frac{1}{2}}\right].$$

Wyngaard (1971) shows that (21) can be recast in the form

$$\Sigma = -3{\cdot}10\,Pr^{-2}\int_0^\infty x^4\tilde{\Gamma}(x)\,dx, \tag{22}$$

where x and $\tilde{\Gamma}$ are the Kolmogorov scaled wavenumber and scalar spectrum. Substituting $\tilde{\Gamma} = -x\,d\tilde{\Psi}/dx$ into (22) and integrating by parts gives

$$\Sigma = -15{\cdot}5\,Pr^{-2}\int_0^\infty x^4\tilde{\Psi}(x)\,dx. \tag{23}$$

Figure 10 gives Σ as a function of Pr as calculated from models for the scalar spectrum as well as from data. The solid and dashed curves are from models 4 and 2 of Hill (1978) using the parameters he obtains by fitting these models to the data of Champagne *et al.* (1977). The model 2 fit gives $q = 4$ whereas the model 4 fit gives $q = 5$. Both of these values of q exceed the bound $q < 2\sqrt{3}$ given by Gibson (1968). Gibson's bound assumes that Batchelor's effective least-principal rate-of-strain parameter γ is bounded by the root mean square of the instantaneous local values of the least principal rate of strain; this assumption gives the simplest bound. As Gibson points

out, assuming a different criterion will give a different bound to q, e.g. if γ is bounded by the mean of the local least-principal rate of strain then the bounds on q are relaxed. Thus it is possible for measured or model-fit values of q to exceed Gibson's bound.

Model 2, which gives the dashed curve, tends to Batchelor's spectrum for large Pr, namely

$$\tilde{\Gamma}(x) = qx^{-1}\exp(-qx^2/Pr), \tag{24}$$

which is equivalent to (16). Equations (24) and (22) give $\Sigma = -1{\cdot}55/q$. For very large Pr model 4 tends to the Kraichnan–Mjolsness form

$$\tilde{\Gamma}(x) = qx^{-1}(1+cx)\exp(-cx),$$

$$c = (6q/Pr)^{\frac{1}{2}},$$

which gives $\Sigma = -2{\cdot}58/q$. For very small Pr model 2 tends to the Corrsin–Pao spectrum, namely

$$\tilde{\Gamma}(x) = \beta x^{-\frac{5}{3}}\exp[-(3\beta/2Pr)\,x^{\frac{4}{3}}]. \tag{25}$$

Equations (25) and (22) give $\Sigma = -1{\cdot}12Pr^{\frac{1}{3}}\beta^{-\frac{2}{3}}$, which implies that $\Sigma \to 0$ as $Pr \to 0$. In the limit of very small Pr, Gibson's k^{-3} inertial–diffusive range spectrum gives values of Σ that are much less than the zero value from models 2 and 4; Clay (1973) obtains $\Sigma \simeq -0{\cdot}52$ for $Pr < 10^{-2}$ from Gibson's k^{-3} spectrum. For $Pr = 0{\cdot}018$ Howells' model gives a value $\Sigma = -0{\cdot}24$, which is insensitive to the value of the parameter q.

Using (23) and Clay's $Pe = 1120$ data gives $\Sigma = -0{\cdot}46$ for $Pr = 0{\cdot}018$, in good agreement with Clay's determination of Σ using the same method. This Σ value is in better agreement with $\Sigma \simeq -0{\cdot}52$ from Gibson's k^{-3} spectrum than with the other models in figure 10. It is obvious from figures 7 or 8 that $\Sigma = -0{\cdot}24$ from Howells' model will be larger than the value $\Sigma = -0{\cdot}46$ from Clay's $Pe = 1120$ data because $x^4\tilde{\Psi}(x)$ has its maximum at about $x = 0{\cdot}05$ where the $Pe = 1120$ data exceed Howells' model by almost a factor of two. The previously mentioned Péclet-number effect implies that the $Pe = 1120$ data exceed what would be obtained from a large-Pe measurement of $\tilde{\Psi}$ in the vicinity of $x = 0{\cdot}05$. Thus $\Sigma = -0{\cdot}46$ must be viewed as a lower bound for $Pr = 0{\cdot}018$ and $Pe \gg 1120$. Unfortunately, no Σ value is available from Clay's $Pe = 4860$ data because this run does not extend to large enough wavenumbers to resolve the $x^4\tilde{\Psi}$ curve. If $\Sigma \geqslant -0{\cdot}46$ for $Pr = 0{\cdot}018$ and $Pe \gg 1120$ then Howells' model and models 2 and 4 remain competitive with Gibson's k^{-3} prediction for obtaining reasonable Σ values. A definitive selection between the various models for $Pr \ll 1$ must await measurements of $\tilde{\Psi}(x)$ for $Pe \gg 1120$ that are accurate to high enough wavenumbers to resolve the $x^4\tilde{\Psi}(x)$ curve.

Values of Σ obtained using (23) and the atmospheric temperature spectra ($Pr = 0{\cdot}72$) of Williams & Paulson (1977) and Champagne *et al.* (1977) are shown on figure 10. The Champagne *et al.* data had no noise subtraction and had a signal-to-noise ratio of unity at $x = 1$; the upper limit of integration in (23) was truncated at $x = 1{\cdot}3$; the resulting value $\Sigma = -0{\cdot}62$ is probably an underestimate because of the noise contributions. The Williams & Paulson data had a noise subtraction; the upper limit in (23) was set to $x = 1{\cdot}5$ with $\Psi(x = 1{\cdot}5) = 0$; the resulting values were $\Sigma = -0{\cdot}59$ for their 9-run average spectrum and $\Sigma = -0{\cdot}48$ for one of their low-noise spectra. The discrepancy between these Σ values illustrates the sensitivity of the $x^4\Psi$ spectrum to the presence of noise, noise subtraction procedures, and other instrumental problems. A

direct measurement of Σ in air over the ocean was made by Clay (1973) with a wire anemometer and a wire thermometer separated by one-half the Kolmogorov microscale. Because of the salt-spray contamination effect discussed by Schmitt, Friehe & Gibson (1978), this and other over-ocean measurements might not be reliable.

Clay (1973) used (23) to obtain $\Sigma = -0{\cdot}29$ from a water-tunnel ($Pr = 7{\cdot}0$) measurement of Ψ. However, his direct measurement of Σ showed no tendency to a constant Σ value with decreasing probe separation; at the smallest probe separation he obtained $\Sigma = -0{\cdot}32$. Consequently, his results indicate that $-0{\cdot}32$ is an upper bound for $Pr = 7{\cdot}0$.

It must be noted that the integral in (23) obtains its dominant contributions from well within the dissipation range where the behaviours of Howells' model and models 2 and 4 are speculative and where measurements of scalar spectra are difficult. The shape of the scalar spectrum in the dissipation range probably depends on Reynolds number because of the increasing small-scale intermittency with increasing Reynolds number. Thus, even if the Péclet number is large enough to attain good separation between the variance-containing and dissipation ranges of the scalar spectrum, the correlation Σ will probably vary with Reynolds number.

5. Conclusion

Howells' equation (1) is simplified for the case of large-Péclet-number turbulence and generalized by making Batchelor's constant, q, a parameter to be chosen by comparison with observations.

Howells' model is compared with the data obtained by Champagne *et al.* (1977) ($Pr = 0{\cdot}72$) and by Grant *et al.* (1968) ($Pr = 9{\cdot}2$). This comparison shows that the model predicts a transition from the inertial–convective range to the viscous–convective range which lies at a wavenumber much higher than the experiments indicate. Consequently, Howells' model does not compare favourably for large and intermediate Prandtl numbers at wavenumbers greater than those wavenumbers in the inertial–convective range.

Since the transitional wavenumber between the inertial–convective to viscous–convective range is too large, it is suggested, but not proven, that for $Pr \ll 1$ the model places the transition from the inertial–diffusive range to the viscous–diffusive range at too high a wavenumber. Despite this large transitional wavenumber, the model predicts that for $Pr = 0{\cdot}018$ the viscous–diffusive range begins at such a wavenumber that the $k^{-\frac{17}{3}}$ inertial–diffusive power law does not appear. On the basis of a different model spectrum, Hill (1978) also predicted that the inertial–diffusive range is very limited in extent for $Pr = 0{\cdot}018$ and that a convincing observation of the inertial–diffusive range would require $Pr \simeq 10^{-3}$.

The temperature spectra for two Péclet numbers ($Pe = 1120$, 4860) measured in mercury ($Pr = 0{\cdot}018$) by Clay (1973) are compared with Howells' model. The comparison of the model with the $Pe = 1120$ run, as well as comparison of the $Pe = 4860$ run with the $Pe = 1120$ run, suggests that the $Pe = 1120$ run is of too small a Péclet number for an inertial–convective range to appear; this same conclusion was reached by Hill (1978). It is not known whether the $Pe = 4860$ data is of large enough Péclet number for a true inertial–convective range to appear because the measured β values do not level off with increasing Péclet number. Despite this problem, Howells' model

and Clay's data agree for the wavenumbers $0{\cdot}02 < x < 0{\cdot}05$ for the $Pe = 1120$ data and $x > 0{\cdot}01$ for the $Pe = 4860$ data.

The $Pe = 1120$ spectrum exceeds the model for $x > 0{\cdot}05$; agreement would require $b = 1{\cdot}5$, which is not possible for the values of β and α used here. It is noted that, if the Péclet number is so small that close proximity of variance-containing and dissipation ranges causes the dissipation spectrum to be reduced near its peak, then the tail of the scaled dissipation spectrum is increased relative to a very-large-Péclet-number measurement because the area under the one-dimensional scaled dissipation spectrum must always be $\frac{1}{6}Pr$. Howells' model is used to show that this Péclet-number effect is sufficient to explain why the $Pe = 1120$ data exceeds the model spectrum for $x > 0{\cdot}05$.

Clay (1973) reports observing two inertial–diffusive range power laws, k^{-3} and $k^{-\frac{1}{3}2}$. The shape of the function $x^3\hat{\Psi}(x)$ near the maximum, as determined from the model, suggests that a convincing observation of a k^{-3} power law would require this power law to be observed over a much wider range of wavenumbers. The $k^{-\frac{1}{3}7}$ power law is observed at wavenumbers within the viscous range of the energy spectrum; at these wavenumbers the Batchelor *et al.* (1959) prediction in equation (20) does not give a $k^{-\frac{1}{3}7}$ power law. Consequently, the observed $k^{-\frac{1}{3}7}$ behaviour cannot be that predicted by Batchelor *et al.* It seems that further high-Péclet-number experiments are needed to adequately resolve the nature of the inertial–diffusive range.

The strain-rate scalar-dissipation correlation, Σ, is calculated from Howells' model for $Pr = 0{\cdot}018$ and compared with Clay's $Pe = 1120$ data. The model value $\Sigma = -0{\cdot}24$ is greater than that from the data $\Sigma = -0{\cdot}48$, but the previously mentioned Péclet-number effect is shown to imply that Σ from a $Pe \gg 1120$ measurement would be greater than $\Sigma = -0{\cdot}48$ from the $Pe = 1120$ data. Atmospheric surface layer temperature spectra and models 2 and 4 of Hill (1978) are also used to estimate Σ.

The author is indebted to J. P. Clay and F. H. Champagne for their helpful discussions.

REFERENCES

BATCHELOR, G. K. 1959 Small-scale variation of convected quantities like temperature in turbulent fluid. Part 1. General discussion and the case of small conductivity. *J. Fluid Mech.* **5**, 113–133.

BATCHELOR, G. K., HOWELLS, I. D. & TOWNSEND, A. A. 1959 Small-scale variation of convected quantities like temperature in turbulent fluid. Part 2. The case of large conductivity. *J. Fluid Mech.* **5**, 134–139.

CHAMPAGNE, F. H., FRIEHE, C. A., LARUE, J. C. & WYNGAARD, J. C. 1977 Flux measurements, flux-estimation techniques, and fine-scale turbulence measurements in the unstable surface layer over land. *J. Atmos. Sci.* **34**, 515–550.

CLAY, J. P. 1973 Turbulent mixing of temperature in water, air and mercury. Ph.D. thesis, University of California at San Diego.

GIBSON, C. H. 1968 Fine structure of scalar fields mixed by turbulence. II. Spectral theory. *Phys. Fluids* **11**, 2316–2327.

GRANT, H. L., HUGHES, B. A., VOGEL, W. M. & MOILLIET, A. 1968 The spectrum of temperature fluctuations in turbulent flow. *J. Fluid Mech.* **34**, 423–492.

HILL, R. J. 1978 Models of the scalar spectrum for turbulent advection. *J. Fluid Mech.* **88**, 541–562.

HOWELLS, I. D. 1960 An approximate equation for the spectrum of a conserved scalar quantity in a turbulent fluid. *J. Fluid Mech.* **9**, 104–106.

McConnell, S. 1976 The fine structure of velocity and temperature measured in the laboratory and atmospheric marine boundary layer. Ph.D. thesis, University of California at San Diego.

Pao, Y. H. 1965 Structure of turbulent velocity and scalar fields at large wavenumbers. *Phys. Fluids* **8**, 1063–1075.

Schmitt, K. F., Friehe, C. A. & Gibson, C. H. 1978 Humidity sensitivity of atmospheric temperature sensors by salt contamination. *J. Phys. Oceanog.* **8**, 151–161.

Williams, R. M. & Paulson, C. A. 1977 Microscale temperature and velocity spectra in the atmospheric boundary layer. *J. Fluid Mech.* **83**, 547–567.

Wyngaard, J. C. 1971 The effects of velocity sensitivity on temperature derivative statistics in isotropic turbulence. *J. Fluid Mech.* **48**, 763–769.